Structural Assessment of Frame Design of 40-ft ISO LNG Tank under High and Low Cycle Load Conditions

Procjena strukturalne nosivosti okvira ISO LNG spremnika od 40 stopa pri uvjetima visokocikličkog i niskocikličkog opterećenja

Tuswan Tuswan
Universitas Diponegoro
Faculty of Engineering
Department of Naval Architecture
Semarang, Indonesia
E-mail: tuswan@lecturer.undip.ac.id

Denis Paskal
PT. Marcopolo Shipyard
Batam, Indonesia
E-mail: denispaskal@alumni.undip.ac.id

Ocid Mursid
University of Strathclyde
Department of Naval Architecture, Ocean and Marine Engineering
Glasgow, United Kingdom
E-mail: ocid-mursid@strath.ac.uk

Alfiy Alfatarizqi
Institut Teknologi Sepuluh Nopember
Department of Marine Engineering
Surabaya, Indonesia
E-mail: alfiyalfatarizqi.research@gmail.com

Hartono Yudo*
Universitas Diponegoro
Faculty of Engineering
Department of Naval Architecture
Semarang, Indonesia
E-mail: hartonoyudo@lecturer.undip.ac.id

DOI 10.17818/NM/2025/2.5
UDK 622.324:629.545
622.242.6:622.324
Original scientific paper / *Izvorni znanstveni rad*
Paper received / *Rukopis primljen:* 15. 4. 2025.
Paper accepted / *Rukopis prihvaćen:* 2. 9. 2025.

Abstract

As a leading global exporter of liquefied natural gas, Indonesia faces substantial logistical challenges in distributing LNG, primarily due to its archipelagic nature. As the primary distribution component, the strength and durability of the LNG ISO tank design for the Mini LNG Carrier is paramount because it must withstand the multifaceted and rigorous demands of multimodal operations spanning land and sea environments. This study examines the fatigue performance of 40-ft ISO LNG tank frame configurations under stationary and dynamic operational loads to obtain optimum strength-to-weight savings. Finite element analysis investigates the fatigue life of 4 proposed LNG tank frame designs under high-cycle and low-cycle conditions, adhering to the ASME and ISO 1496-3 standards guidelines. It can be found that the elimination of longitudinal, vertical, and horizontal frames can effectively reduce stress and displacement and reach 6% total weight saving. The study conclusively shows that in both low and high cycle loading, the fatigue damage factor (FDF) values are below the critical threshold, indicating all proposed frame designs likely achieve a 20-year service life.

KEY WORDS

ISO LNG tank
frame design
fatigue analysis
finite element analysis
low cycle

Sažetak

Indonezija, kao jedan od vodećih svjetskih izvoznika ukapljenog prirodnog plina, suočava se s ozbiljnim logističkim izazovima u distribuciji LNG-a, ponajprije zbog svojega otočnog geografskog položaja. S obzirom na to da je ISO spremnik za LNG ključna komponenta distribucijskog sustava Mini LNG Carrier brodova, njegova čvrstoća i trajnost imaju presudnu važnost jer mora izdržati višestruke i rigorozne zahtjeve multimodalnih operacija na kopnu i moru. Ovo istraživanje ispituje ponašanje okvira ISO LNG spremnika od 40 stopa u pogledu zamora materijala pri stacionarnim i dinamičkim opterećenjima, s ciljem optimizacije omjera čvrstoće i mase. Primjenom metode konačnih elemenata procijenjen je vijek trajanja pri zamoru za četiri predložena okvira spremnika, u uvjetima visokocikličkog i niskocikličkog opterećenja, a u skladu sa smjernicama standarda ASME i ISO 1496-3. Rezultati pokazuju da uklanjanje uzdužnih, vertikalnih i horizontalnih okvira može značajno smanjiti naprezanja i pomake te ostvariti ukupnu uštedu mase od 6%. Zaključuje se da su u svim razmatranim uvjetima opterećenja vrijednosti faktora oštećenja zamorom ispod kritične granice, što potvrđuje da svi predloženi okviri LNG spremnika vjerojatno mogu postići radni vijek od 20 godina.

KLJUČNE RIJEČI

ISO LNG spremnik
okviri
analiza zamora
metoda konačnih elemenata
niskocikličko opterećenje

1. INTRODUCTION / *Uvod*

Liquefied Natural Gas (LNG) has emerged as a globally favoured energy source due to its efficiency and environmental advantages [1]. LNG is produced by cooling natural gas to -160°C, significantly reducing its volume, allowing it to expand 600 times when vaporized [2,3]. Compared to coal or oil, LNG emits substantially fewer pollutants, rendering it a cleaner and more viable fuel option for maritime applications while

* Corresponding author

also reducing overall fuel costs [4]. Although LNG possesses a lower energy density than diesel or Heavy Fuel Oil (HFO), it delivers comparable power with reduced consumption and is approximately 60% less expensive than HFO [5,6]. However, utilizing LNG necessitates larger storage tanks with advanced insulation to accommodate its lower density and maintain its cryogenic state. Environmentally, LNG reduces CO2 emissions by nearly 20%, decreases NOx emissions by 85-90%, and virtually eliminates SOx emissions, aligning with MARPOL Annex VI [7]. Additionally, LNG supports domestic policies such as Indonesia's Government Regulation No. 55 of 2009, which mandates that 25% of natural gas output be utilized nationally [8].

The distribution of LNG to end-users is predominantly executed through three methods: pipeline transport, delivery by tanker trucks, and shipping via tank containers [9]. Primary LNG receiving facilities, which manage LNG delivered by ships, are classified into onshore terminals and offshore installations, known as Floating Storage and Regasification Units (FSRU) [10]. In Indonesia, an archipelagic nation and a significant global supplier of LNG, the logistics of LNG delivery present considerable challenges. To address these issues, the National Development Planning Agency (BAPPENAS) has integrated the development of Mini LNG Carriers into the National Priority Program for the marine sector, covering the period from 2020 to 2024 [11].

LNG is transported using various types of pressurized tanks, including membrane, Moss (spherical), and prismatic (SPB) tanks, each possessing distinct characteristics for LNG containment and transportation. Concurrently, Wang and Qian [12] investigated the effects of fluid inertia forces on stress distribution across the frames and shells of tank containers under different loading conditions. In a similar context, several studies conducted finite element simulations to understand the response of LNG tank containers to inertia forces [13,14] and dynamic sloshing forces on LNG tanks [15-19]. Significant design modifications included the elimination of saddle supports and bottom frames and the increase in the thickness of vertical frames.

ISO tanks are specialized containers designed to efficiently transport liquids and gases, featuring a robust construction with an inner shell, outer shell, and frame structure engineered to meet ASME standards [20,21]. Research on LNG ISO tanks has focused on their design and structural assessment through numerical simulations, particularly for 20-ft and 40-ft configurations. For 20-ft LNG ISO tanks, initial studies by Muttaqie et al. [22] utilized finite element simulations based on ISO 1496-3 [23] to evaluate performance under operational loads. Their work established a foundation for assessing the structural integrity of these tanks under standard conditions. In parallel, significant research has been conducted on 40-ft LNG ISO tanks. Marpaung et al. [24] analyzed a 40-ft tank under various loading conditions outlined in ISO 1496-3, identifying the lower-end frame as the region experiencing the highest stress levels. Similarly, Purnamasari et al. [25] investigated the structural integrity of a 40-ft LNG ISO tank frame, focusing on stacking, lifting, and racking loads. Their findings highlighted stacking and longitudinal racking as critical operational conditions that challenge the tank's structural limits.

Additionally, Lee et al. [26] noted that a 40-ft ISO tank, when 90% full load, weighs approximately 18 tons, leading to stress concentration issues. This underscores the importance of fatigue life prediction to address fatigue intensity caused by these stress concentrations. More recently, Tuswan et al. [27] advanced the design of 40-ft LNG ISO tanks by employing topology optimization. Their approach achieved a significant weight reduction of 18.4–37.3% while maintaining acceptable stress levels, enhancing the tank's efficiency without compromising structural integrity. This progression of research, from establishing benchmarks for 20-ft tanks to optimizing the design of 40-ft tanks, demonstrates a clear focus on improving structural performance, reducing weight, and ensuring reliability under demanding operational conditions.

In operational environments involving land and maritime transport of liquefied natural gas LNG, ISO tank containers are subjected to cyclic stresses arising from repeated loading and unloading cycles, potentially culminating in structural degradation and failure over prolonged service life. Consequently, comprehensive fatigue assessment of LNG ISO tank frames under both low- and high-cycle loading regimes is imperative to safeguard structural integrity and ensure the secure containment of LNG cargo. Although ISO tank containers conform to standardized dimensions and construction protocols to facilitate intermodal compatibility, LNG-specific variants permit tailored frame architectures. Manufacturer-specific engineering decisions, operational demands, and compliance with jurisdiction-dependent regulatory frameworks typically inform such modifications. Despite the critical implications for safety and reliability, the extant literature reveals a paucity of investigations into fatigue behaviour for 40-ft LNG ISO tanks, particularly concerning the impact of diverse frame configurations, a notable oversight given the escalating global reliance on LNG as a transitional energy source. The present study endeavours to bridge this scholarly lacuna by employing FEA to elucidate the effects of varying frame configurations on the fatigue endurance of 40-ft LNG ISO tanks under representative operational loading scenarios. Specifically, four customized frame designs are evaluated through nonlinear fatigue simulations, with variations in overall frame utilization, while prioritizing high- and low-cycle fatigue conditions as delineated in the ISO 1496-3 standard.

2. MATERIALS AND METHODS / *Materijali i metode*

2.1. Framework of Fatigue Analysis / *Analiza zamora*

Finite element analysis is commonly used in many engineering cases [28]. This study utilized FEA software to perform fatigue analysis. The methodology began by developing a 3D model of the tank and container, after which parameters and loading conditions were established per ISO 1496-3 standards [23]. The meshing process was verified by ensuring the error margin did not exceed 5%, allowing the simulation to proceed precisely based on the defined study variables. Upon completion of the simulation, stress range values for each model variation and loading scenario were obtained. These values were subsequently used to perform fatigue analysis calculations, which involved determining stress amplitude, stress factor, the cycle count exponent, and permissible design cycles to derive the fatigue damage factor. The results of these calculations are graphically presented in Fig. 1, offering a clear foundation for the study's findings and conclusions.

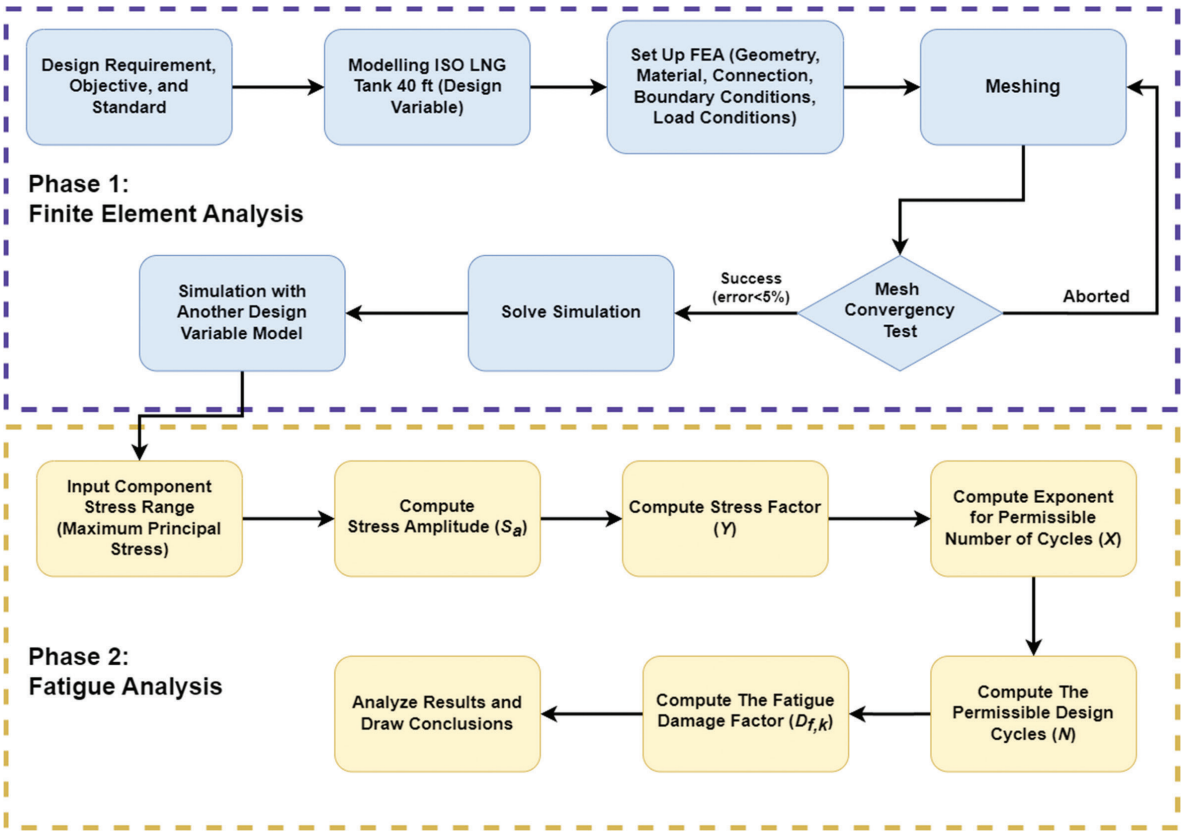

Figure 1 Fatigue flowchart for 40 ft LNG ISO tank
Slika 1. Dijagram toka analize zamora za LNG ISO spremnika od 40 stopa

Source: Authors

2.2. Geometry of ISO Tank Model / *Geometrija modela ISO spremnika*

The ISO tank type consists of fundamental elements: bakelite, baffle, ring stiffener, corner casting, frame structure, and inner and exterior shells developed based on past studies by the National Research and Innovation Agency (BRIN) [22]. The LNG ISO tank design guarantees adherence to the ASME Section II and ASME Section VIII [20,21]. With parameter definitions shown in Fig. 2, ASME VIII-1 section UG-27 [20] defines the thorough method for computing the minimum required thickness. Fig. 3 also schematically shows a torispherical head.

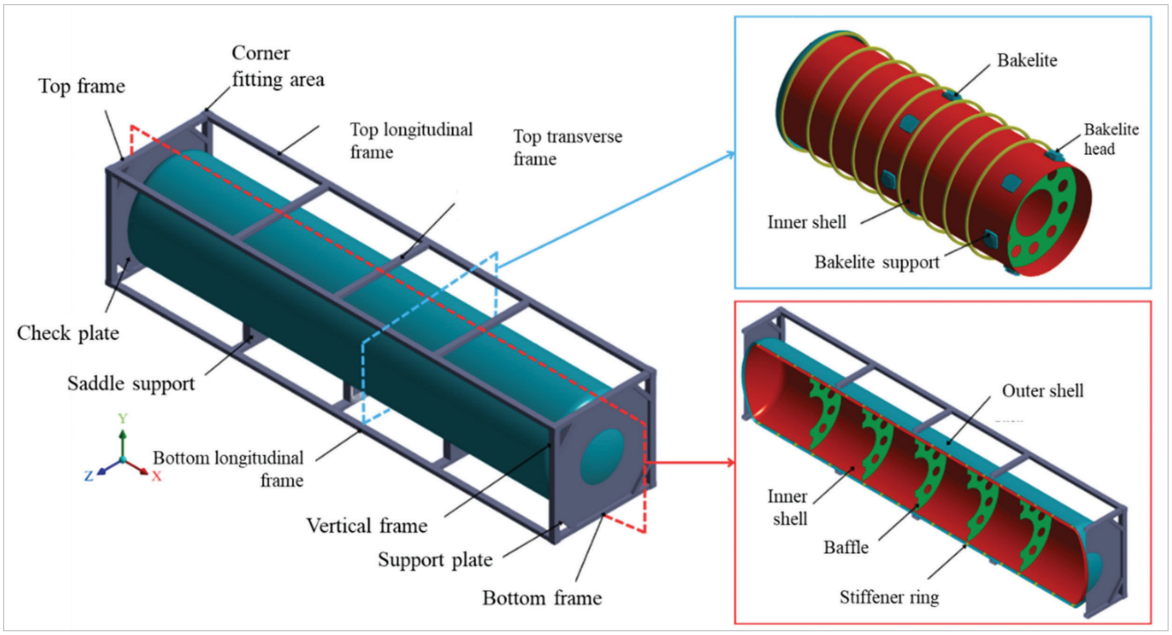

Figure 2 LNG ISO tank geometry detail
Slika 2. Detalji geometrije LNG ISO spremnika

Source: Authors

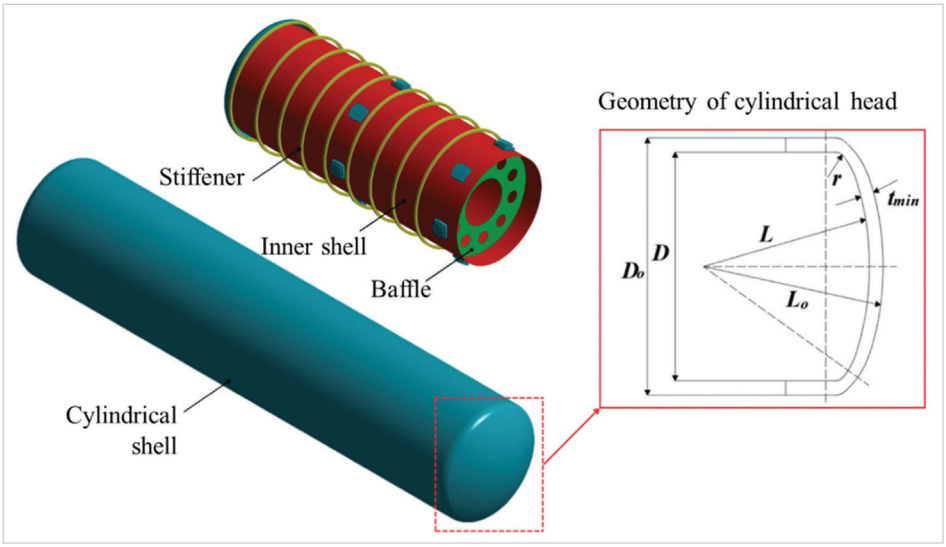

Figure 3 Geometry design of 40-ft LNG ISO tank
Slika 3. Geometrijski projekt LNG ISO spremnika od 40 stopa

Source: Authors

The minimum thickness (*t*) of the pressure vessel is described in Equation 1.

$$t = \frac{PR}{SE - 0.6P} \quad (1)$$

where *P* represents the internal design pressure, *R* is the internal radius, *S* denotes the permissible stress for stainless steel (SUS 304 L), and *E* indicates the efficiency of the butt joint. For additional details, consult ASME Table UW-12 [20]. Moreover, the computation for the concave side of the toroidal shell at both cylinders ends, as demonstrated in Equations 2 and 3, is based on Section UG-32.

$$t = \frac{PLM}{2SE - P(M - 0.2)} \quad (2)$$

$$M = 0.25\left(3 + \sqrt{\frac{L}{R}}\right) \quad (3)$$

where *R* is the inner radius in mm, and *L* is the inner crown radius in mm.

Meanwhile, paragraph UG-28 Part VIII [20] determines the maximum permissible external pressure on the cylindrical shell. Initially, confirming that the geometry *D0/t* is equal to or greater than 10 is necessary. Following this confirmation, the external pressure chart from Fig. G in ASME Section II, Part D, Subpart 3 [21] is used to derive the *A* value based on the fundamental ratios of *L/D0* and *D0/t*. Upon determining the A value, the corresponding *B* value for the 304L material specification is identified from Fig. HA-3. Ultimately, the highest allowable value is calculated using the *B* value as outlined in Equation 4.

$$p_a = \frac{4B}{3\left(\frac{D}{t}\right)} \quad (4)$$

The computation aligns with UG-29 of ASME Section VIII [20], which addresses establishing the pressure capacity for the ring stiffener on a pressure vessel. At this stage, the methodology assumes the ring stiffener retains its initial dimensions and configuration.

$$B = 0.75\left(\frac{PD}{t + \frac{A_s}{L_s}}\right)/14 \quad (5)$$

where A_s represents the anticipated cross-sectional area of the ring stiffener, L_s is the spacing between stiffeners, and *t* is the shell thickness determined in the prior step. Subsequently, the value of *B* is computed using Equation 5. This *B* value can then be utilized to determine a corresponding *A* value that matches the *B* value derived from the external pressure diagram in ASME Section II, Part D [21].

$$I_s' = [D_0{}^2 L_s(t + \frac{A_s}{L_s})A]/14 \quad (6)$$

$$I = \frac{t_{wh_{wx}{}^3}}{12} \quad (7)$$

Equation 6 was initially used to determine the appropriate moment of inertia for the ring stiffener. A preliminary estimate of the actual moment of inertia for the ring stiffener is then given using Equation 7. These findings suggest that the necessary moment of inertia should be equal to, if not greater than, the actual moment of inertia. The predicted thicknesses for the pressure vessels, according to ASME Section VIII [20], are summarized in Table 1.

Table 1 Pressure vessel thickness result calculated by ASME Section VIII.
Tablica 1. Rezultat izračunate debljine tlačne posude prema ASME Section VIII

Design parameters	Value	Unit
Internal design pressure (P_{int})	1	MPa
External design pressure (P_{ext})	0.8	MPa
Inner tank parameter		
Inner shell thickness (*t*)	7.1	mm
Inner head thickness (*t*)	11.22	mm
Diameter of inner tank (*D*)	2218	mm
Cylindrical length of inner tank (L_{cyl})	11018	mm
Inner crown radius (*L*)	2218	mm
Inner knuckle corner radius (*r*)	221.8	mm
Outer tank parameter		
Outer shell thickness (*t*)	3.95	mm
Outer head thickness (*t*)	6.28	mm
Diameter of outer tank (*D*)	2438	mm
Cylindrical length of outer tank (L_{cyl})	11018	mm
Outer crown radius (*L*)	1950.4	mm
Outer knuckle corner radius (*r*)	243.8	mm

Source: Authors as per [20].

Table 2 Material properties of the LNG ISO tank
Tablica 2. Svojstva materijala LNG ISO spremnika

Materials	Density	Young modulus	Poisson's ratio	Yield strength
	ton/mm^3	N/mm^2	-	N/mm^2
Steel frame	7.85E^{-9}	210,000	0.3	340
SA240Gr304L-PV	7.85E^{-9}	193,000	0.3	175
ISO corner casting	7.85E^{-9}	215,800	0.3	275
Carbon steel ASTM A516	7.75E^{-9}	200,000	0.3	248
Bakelite	1.28E^{-9}	8,300	0.29	55

Source: Authors as per [21,29-32]

The selection of materials for the 40 ft ISO tank is based on the specifications provided in Part II of ASME [21]. The inner tank is constructed using SA240Gr304L-PV material for this application, while the ring stiffener and outer shell are made from carbon steel ASTM A516. The frame structure, including the saddle support, is fabricated from steel. This study uses SUS 304L alloy steel, corresponding to the ASME specification SA 240 Gr 304L-S [21]. The properties of the materials used for the 40 ft ISO tank are detailed in Table 2.

2.3. Boundary Setting & Loading Scheme / *Postavke graničnih uvjeta i shema opterećenja*

This study performed FEA analysis for ISO tanks under high-cycle and low-cycle conditions to evaluate their ability to withstand operational forces and stresses. According to ISO 1496-3 part 3 [23], tank containers for liquids, gases, and pressurized dry bulk must undergo specific tests to ensure durability throughout their service life. Low-cycle conditions simulate a stationary tank, achieved by restricting movement in the 3D model. Specifically, the tank's bottom casting area was fixed in the x, y, and z directions, as indicated by Fig. 4, limiting translation and rotation to establish boundary conditions for modelling. At low-cycle, the external tank pressure was kept constant at 0.101 MPa; the interior tank pressure for the low-cycle assessment was 0.509 MPa, and the dead weight was 34,000 kg. Moreover, in separate simulation cases, high-cycle conditions, representing transit by road, rail, or sea, were simulated by applying accelerations to three corners of the tank. The high-cycle evaluation made use of accelerations of 2 g in the vertical direction (y-axis), 1 g in the transverse direction (z-axis), and 1 g in the longitudinal direction (x-axis) per ISO 1496 standard [23]. Fig. 5 depicts the locations and directions of acceleration applications under high-cycle conditions. These supports are set to restrict rotational and translational movement over all axes on the designated surface.

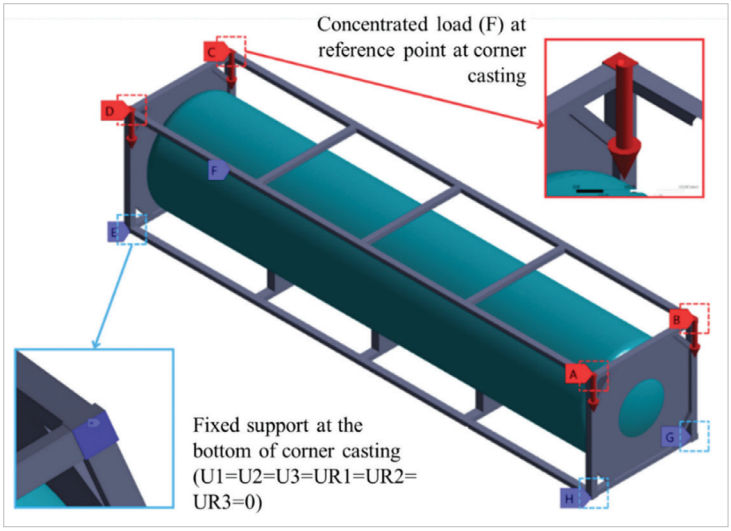

Figure 4 Boundary conditions of ISO tank 40 ft.
Slika 4. Granični uvjeti ISO spremnika od 40 stopa

Source: Authors

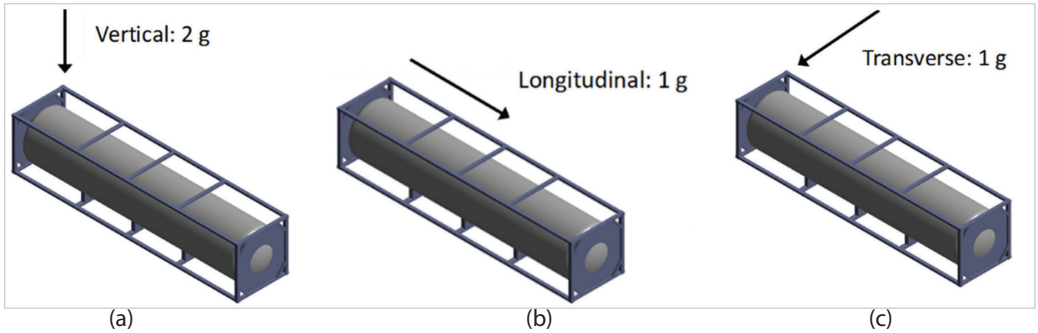

Figure 5 Illustration of acceleration application in high-cycle tests
Slika 5. Kontura primjene ubrzanja u testovima visokocikličkog opterećenja

Source: Authors

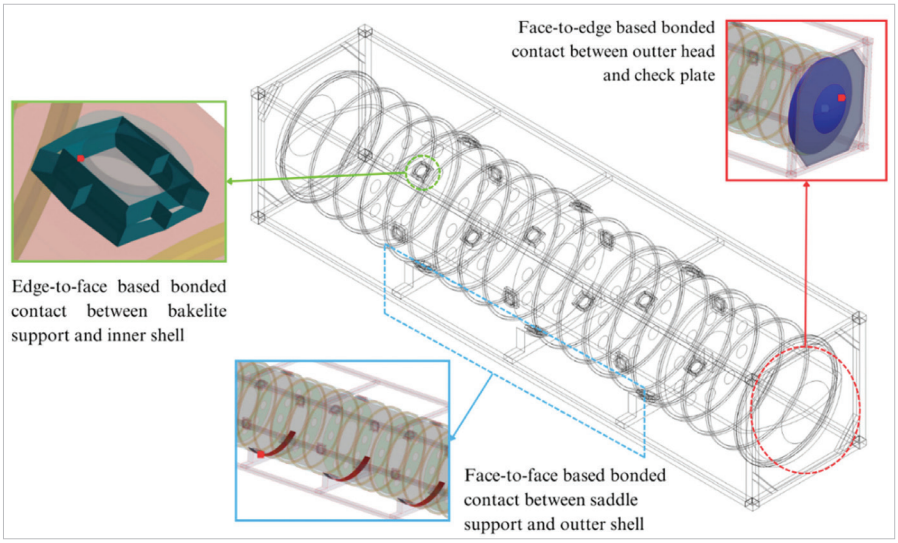

Figure 6 Boundary condition settings
Slika 6. Postavke graničnih uvjeta

Source: Authors

In the connection settings illustrated in Fig. 6, the first zone refers to the connection between the front and rear tanks, which includes a check plate. This reinforcement is crucial in maintaining a strong and dependable link between the components, allowing them to operate effectively under different conditions. The second zone centres on the direct interaction between the cylindrical bottom tank and the saddle. This interface is crucial for creating a steady and consistent connection, promoting effective load distribution. A schematic illustration of these boundary specifications is shown in Fig. 6.

2.4. Mesh Convergence Analysis / *Analiza konvergencije mrežnog modela*

Meshing involves dividing a geometric structure into small, interlinked components called meshes, each characterized by specific shapes and nodes. In the context of finite element analysis, the mesh size is a crucial factor, as it directly impacts the accuracy of the outcomes and the total number of elements required [33]. For this model, the meshing was performed using the ANSYS Meshing tool. To achieve an optimal balance between accuracy and computational efficiency, convergence tests were conducted across mesh sizes ranging from 55 mm to 35 mm, as illustrated in Fig. 7. Shell elements were employed to discretize the model and to assess all loading scenarios. The outcomes of the mesh convergence tests for each loading scenario are displayed in Fig. 8. The tests indicated that a mesh size of 40 mm produced displacement errors below 0.5% and maximum stress errors under 5%. As a result, a mesh size of 40 mm was selected for this study, generating a total of 186,363 elements.

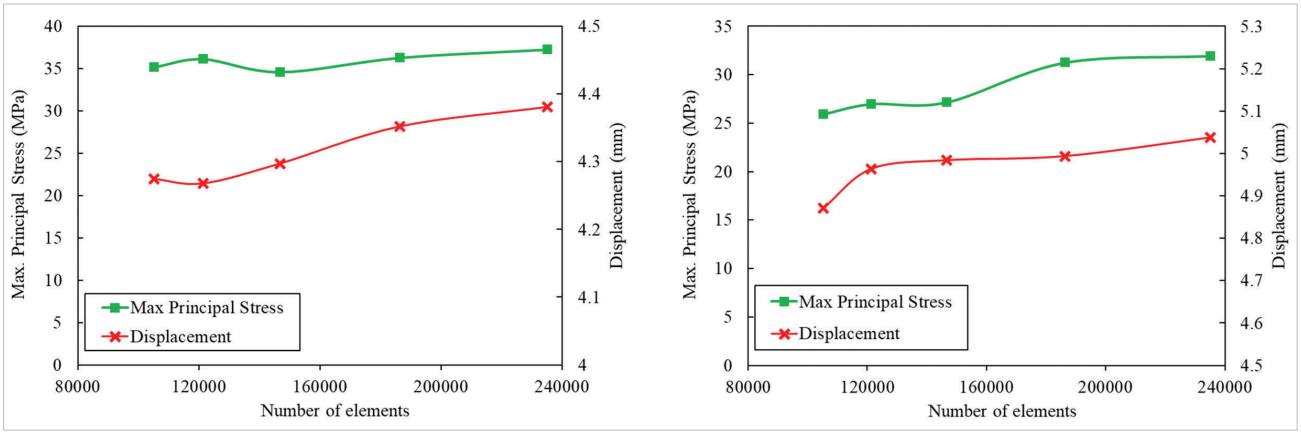

Figure 7 Mesh convergence test on loading scenarios of (a) high-cycle (longitudinal) test, (b) high-cycle (transversal) test
Slika 7. Test konvergencije mrežnog modela za scenarije opterećenja: (a) visokociklički (uzdužni) test, (b) visokociklički (poprečni) test

Source: Authors

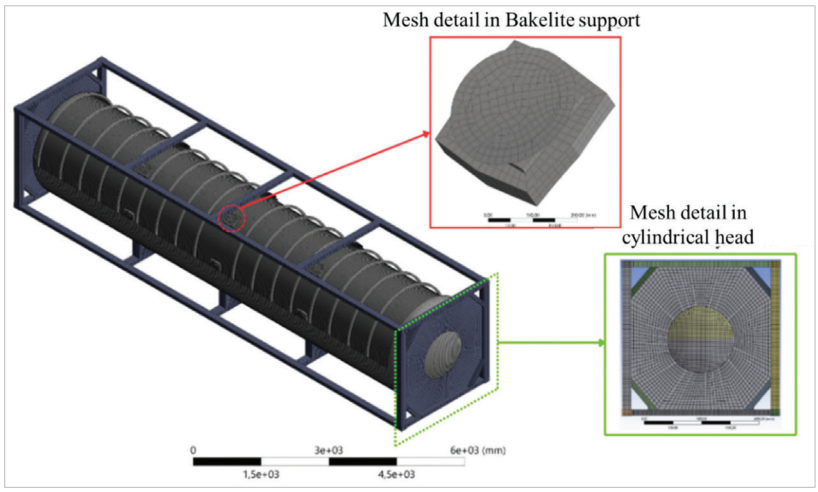

Figure 8 Meshing on the structural frame and LNG ISO tank
Slika 8. Diskretni mrežni model strukturnog okvira i LNG ISO spremnika

Source: Authors

2.5. LNG ISO Tank Design Variable / *Projektne varijable LNG ISO spremnika*

The reference model of the 40 ft LNG ISO tank frame, initially developed by the National Research and Innovation Agency (BRIN) in Surabaya, Indonesia, serves as a benchmark for evaluating structural performance in Mini LNG Carrier applications [25]. It focuses on the arrangement and presence of vertical, longitudinal, and transverse plates, as shown in Table 3. The changes in structure, shown in Fig. 9, involve adding or removing these frames to see how each affects the frame's fatigue performance. The main model, shown in Fig. 9a, uses vertical, longitudinal, and transverse frames to stay strong under the moving loads during LNG transport. The vertical frames are hollow and measure 150x100x10 mm, making them stiffer because they are bigger. The longitudinal and transverse frames are 100x100x10 mm, balancing weight and strength. These sizes are selected to obtain a strong but lightweight structure, which is essential for Mini LNG Carriers. Table 3 lists the frame setups tested, showing how many frames each uses. By removing some frames, the study finds out how each type helps resist repeated loading and prevents fatigue failures. It helps understand how each part of the structure adds to the tank frame's strength and life.

3. STRUCTURAL STRENGTH OF LNG ISO TANK / *Strukturna čvrstoća LNG ISO spremnika*

The analysis of maximum principal stresses in Table 4 and Fig. 10 reveals distinct trends across the LNG ISO tank models, which vary in frame complexity. Under low-cycle stationary conditions, where the tank is fixed at the bottom with constant external pressure of 0.101 MPa, internal pressure of 0.509 MPa, and a 34,000 kg dead weight, stresses in the frame and corner

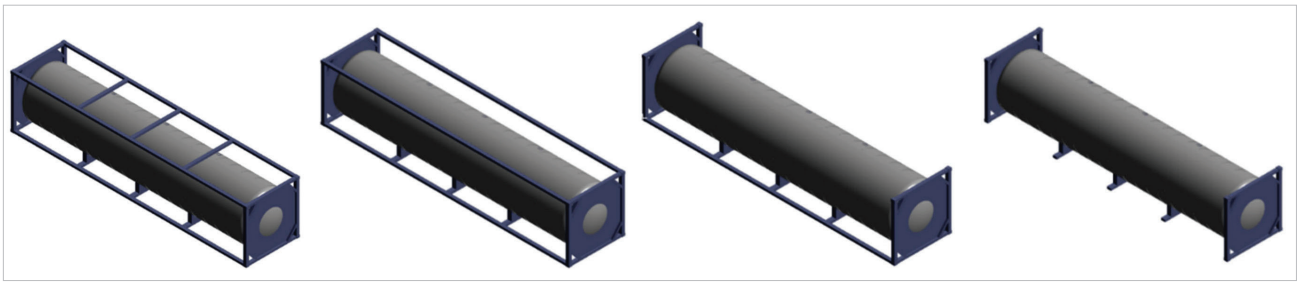

(a) (b) (c) (d)

Figure 9 Designed frame variations: (a) Model A, (b) Model B, (c) Model C, (d) Model D
Slika 9. Varijacije okvira: (a) Model A, (b) Model B, (c) Model C, (d) Model D

Source: Authors

Table 3 Design variables of LNG ISO tank models
Tablica 3. Projektne varijable LNG ISO spremnika

Frame parts	Model A	Model B	Model C	Model D
Vertical frame	4	4	4	4
Bottom longitudinal frame	2	2	2	0
Top longitudinal frame	2	2	0	0
Top transverse frame	3	0	0	0

fittings decrease progressively from Model A to Model D, indicating that simpler frames distribute loads more efficiently to other components. In comparison, pressure vessel stresses remain uniform at 156.54 MPa across all models, likely due to the dominance of internal pressure over frame variations. In high-cycle vertical loading, a similar pattern emerges, with frame and corner stresses being highest in Model A and lowest in Model D. However, vessel stresses are low and comparable, suggesting robust vertical load handling in sparser frames. Conversely, high-cycle longitudinal loading shows Models A, B, and C maintaining moderate frame and lower vessel stresses. However, Model D exhibits significantly elevated values, highlighting potential vulnerabilities in minimal framing under lengthwise forces, possibly due to reduced structural reinforcement. For high-cycle transversal loading, stresses are generally lower overall, decreasing mildly from Model A to D in frames and corners, with minimal vessel stresses, implying adequate lateral stability even in simplified designs. Models C and D appear advantageous for reducing stresses in stationary and vertical/transversal scenarios. Still, Model D's higher longitudinal stresses underscore the need for balanced framing to mitigate risks in multi-directional transit, aligning with ISO 1496 standards for safe transport.

Table 4 Comparison of maximum principal stress on LNG ISO tank design variations

Tablica 4. Usporedba maksimalnog naprezanja pri različitim projektnim varijacijama LNG ISO spremnika

Load scenario	Model	Maximum principal stress (MPa)		
		Frame	Corner fitting	Pressure vessel
Low cycle	Model A	45.25	25.45	156.54
	Model B	32.34	18.21	156.54
	Model C	23.03	4.38	156.54
	Model D	17.06	3.54	156.54
High-cycle (vertical)	Model A	89.70	51.20	25.50
	Model B	64.55	36.49	24.96
	Model C	15.65	8.40	25.05
	Model D	12.46	7.34	23.06
High-cycle (longitudinal)	Model A	36.30	21.85	36.75
	Model B	36.67	19.55	33.68
	Model C	35.99	13.98	33.06
	Model D	96.99	26.73	41.07
High-cycle (transversal)	Model A	31.26	12.35	12.58
	Model B	28.03	12.48	12.55
	Model C	13.18	10.99	12.53
	Model D	12.69	9.58	12.41

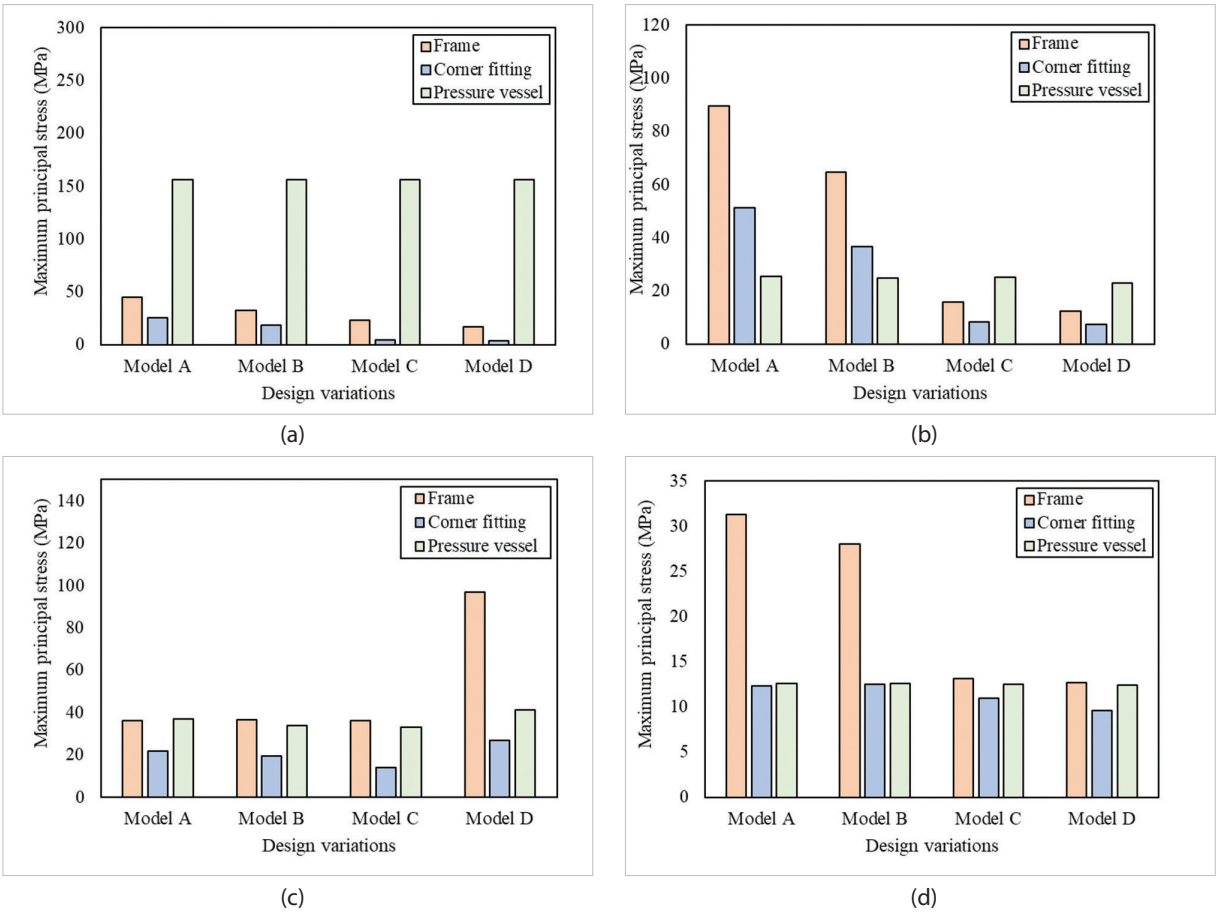

Figure 10 Maximum principal stress values: (a) low-cycle test, (b) high-cycle (vertical) test, (c) high-cycle (longitudinal) test, (d) high-cycle (transversal) test

Slika 10. Vrijednosti maksimalnog glavnog naprezanja: (a) niskociklički test, (b) visokociklički (vertikalni) test, (c) visokociklički (uzdužni) test, (d) visokociklički (poprečni) test

Source: Authors

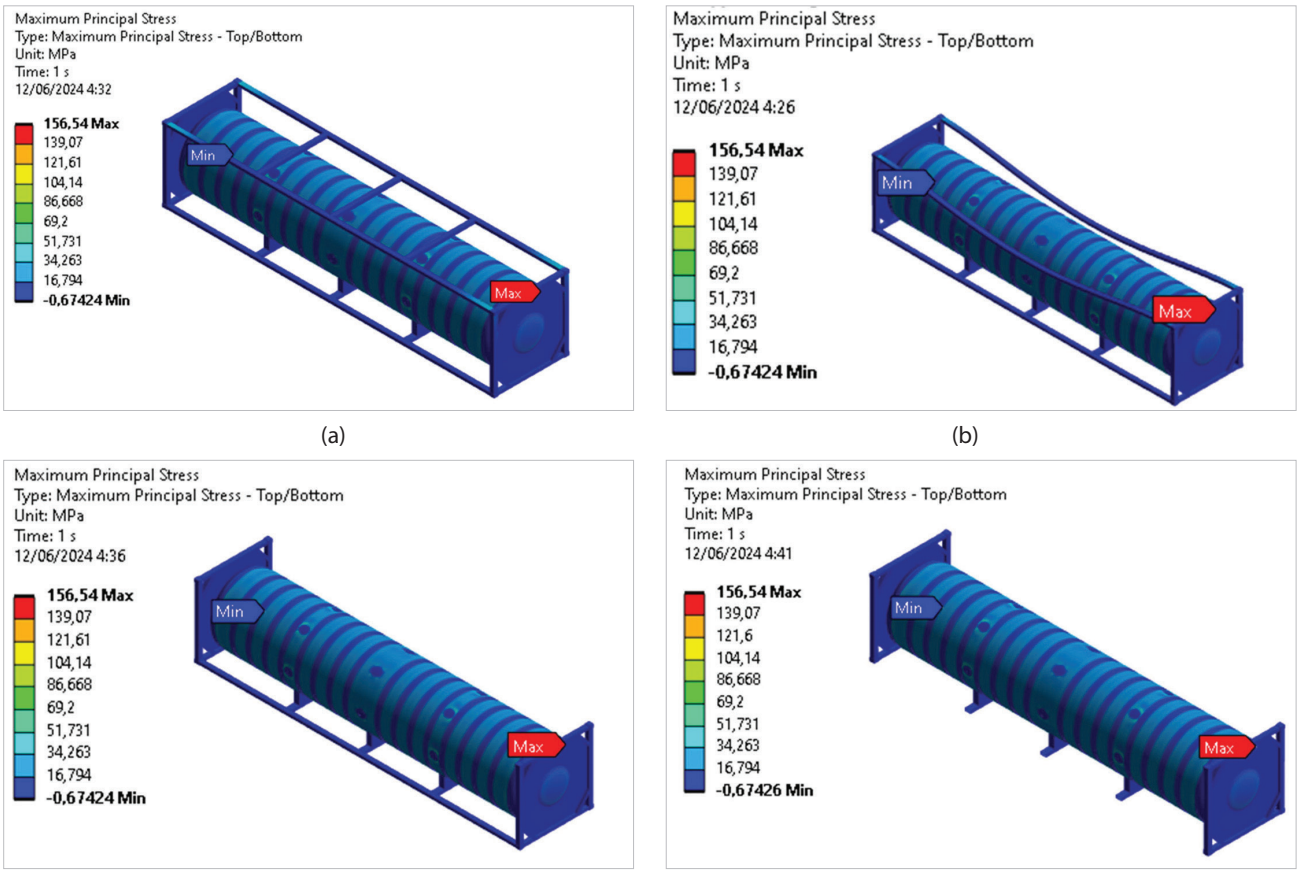

Figure 11 The stress contour under low-cycle test: (a) Model A, (b) Model B, (c) Model C, and (d) Model D

Slika 11. Kontura naprezanja pri niskocikličkom testu: (a) Model A, (b) Model B, (c) Model C, (d) Model D

Source: Authors

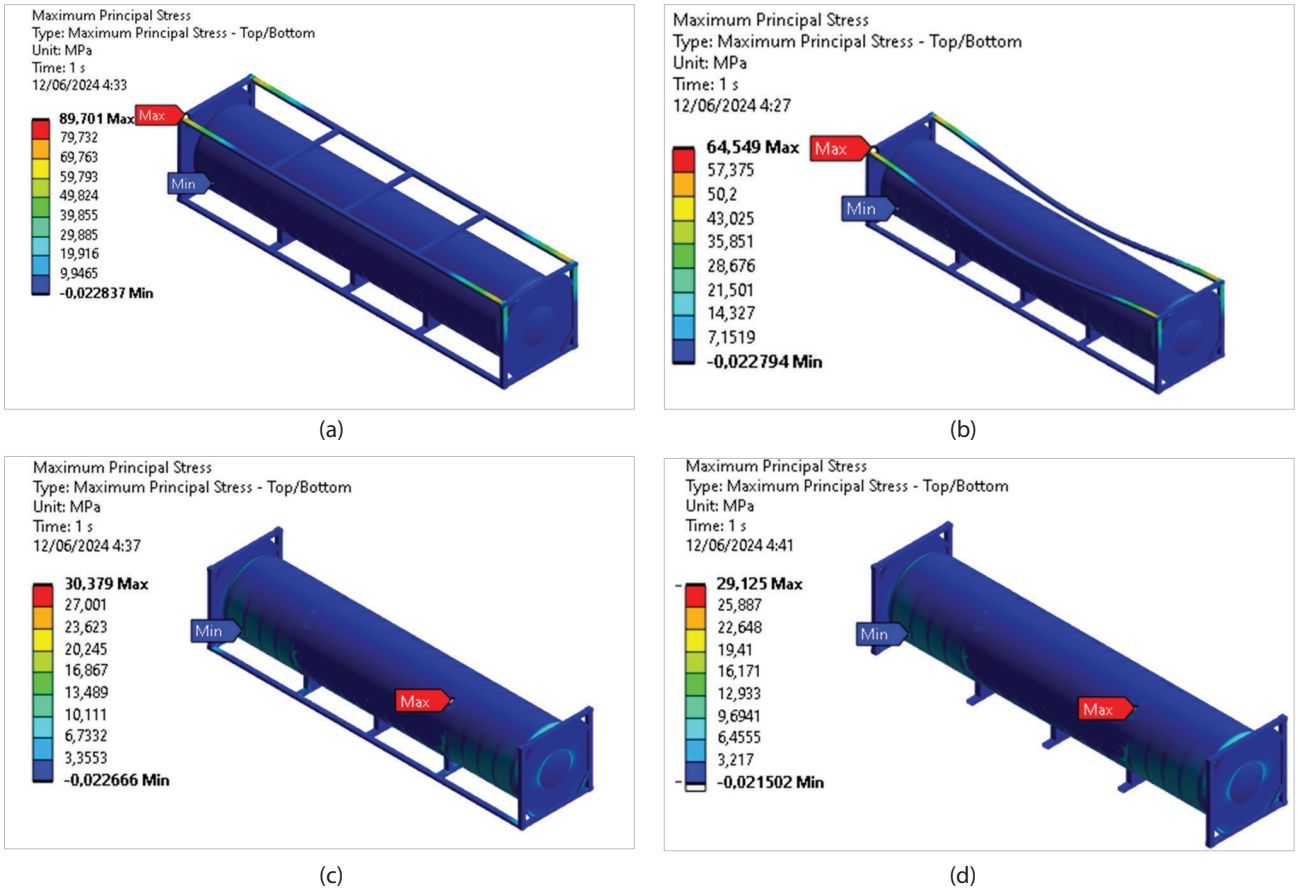

Figure 12 The stress contour under high-cycle (vertical) test: (a) Model A, (b) Model B, (c) Model C, and (d) Model D

Slika 12. Kontura naprezanja pri visokocikličkom (vertikalnom) testu: (a) Model A, (b) Model B, (c) Model C, (d) Model D

Source: Authors

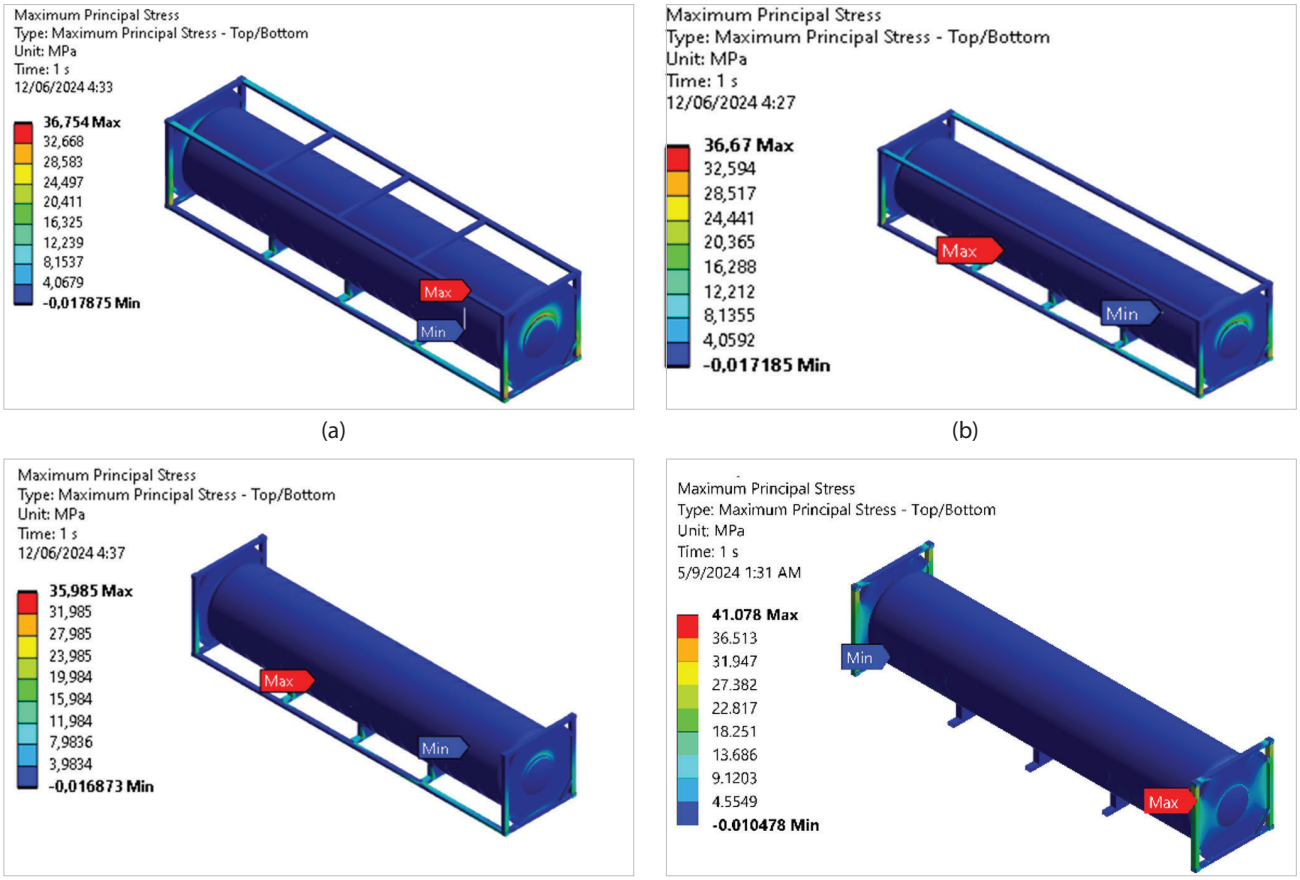

Figure 13 The stress contour under high-cycle (longitudinal) test: (a) Model A, (b) Model B, (c) Model C, and (d) Model D

Slika 13. Kontura naprezanja pri visokocikličkom (uzdužnom) testu: (a) Model A, (b) Model B, (c) Model C, (d) Model D

Source: Authors

The findings indicate that Models C and D generally surpass the more intricate Model A regarding stress reduction under most conditions. In scenarios involving low-cycle stationary loads, frame and corner stresses gradually decrease in Model D. In contrast, the pressure vessel stresses remain constant at 156.54 MPa across all models due to the predominant influence of internal pressure. This pattern is also observed in high-cycle vertical loading, where frame stresses decrease from Model A to Model D, suggesting improved load distribution in the frames without compromising the vessel's integrity. However, high-cycle longitudinal loading in Model D reveals design flaws, pointing to potential risks from insufficient reinforcement against bending loads. Transverse loading results in consistently low stresses, indicating strong lateral performance even in simpler designs. Stress contours depicted in Figures 11-14 visually corroborate these trends, showing that concentrated stress hotspots in complex frames shift to more diffused or end-specific peaks in simpler ones. Overall, Model C is identified as the optimal choice, effectively minimizing stresses across different transit modes according to ISO 1496, while avoiding the longitudinal weaknesses seen in Model D.

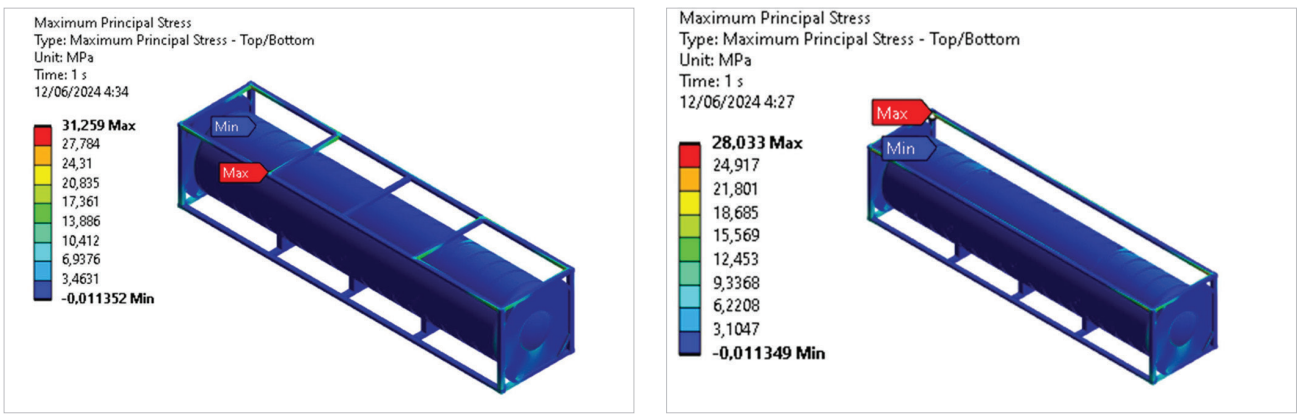

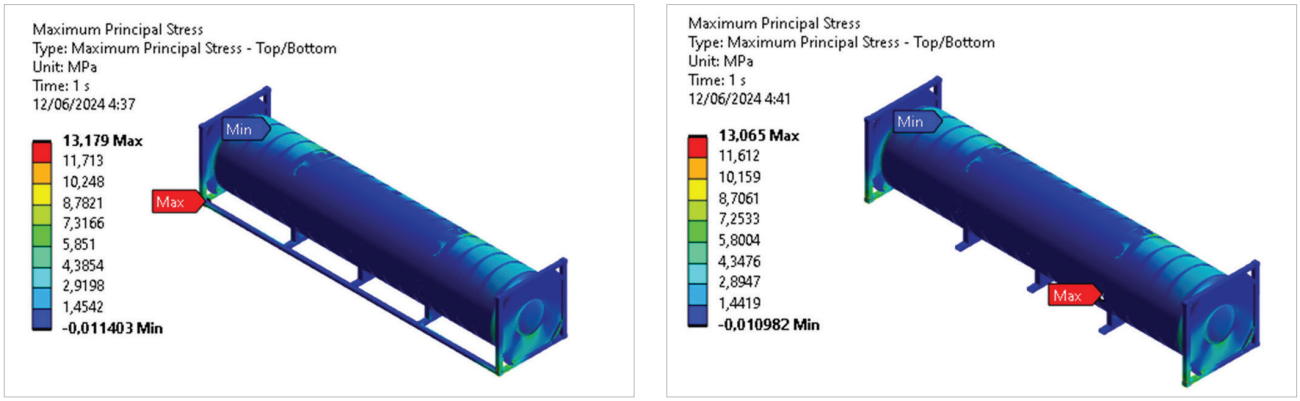

(c) (d)

Figure 14 The stress contour under high-cycle (transversal) test: (a) Model A, (b) Model B, (c) Model C, and (d) Model D

Slika 14. Kontura naprezanja pri visokocikličkom (poprečnom) testu: (a) Model A, (b) Model B, (c) Model C, (d) Model D

Source: Authors

The structural evaluation of LNG ISO tank frame variations demonstrates that simpler designs, particularly Models C and D, generally yield lower maximum stresses and displacements than more complex models such as Model A, promoting material efficiency and reducing fatigue risks during stationary and transit conditions. Under low-cycle stationary loads, frame displacements drop, reflecting better load distribution in structural frames. High-cycle vertical and transversal accelerations show similar trends, with frame stresses and displacements minimizing in Models C and D, ensuring stability under inertial forces. However, longitudinal high-cycle loading reveals Model D's limitation, with elevated stress and displacement due to absent reinforcements. It can also be found that gross weights offer up to 6% savings.

Table 5 Comparison of maximum displacement under different model variations

Tablica 5. Usporedba maksimalne istisnine pri različitim varijacijama modela

Model	Gross weight (R) (ton)	Displacement (mm)			
		Low cycle	High cycle (vertical)	High cycle (longitudinal)	High cycle (transversal)
Model A	35.90	20.26	40.42	4.36	4.99
Model B	35.61	14.11	28.12	3.73	7.65
Model C	34.69	2.24	1.03	1.98	0.52
Model D	33.75	2.25	0.90	2.45	0.51

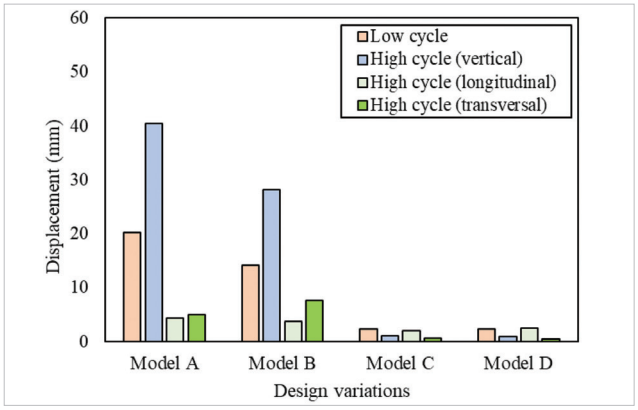

Figure 15 Maximum displacement at different loading scenarios

Slika 15. Maksimalna istisnina pri različitim scenarijima opterećenja

Source: Authors

4. FATIGUE ANALYSIS OF DESIGN VARIATIONS / *Analiza zamora pri različitim projektnim varijacijama*

The highest stress values from FEA define the computations of the fatigue analysis. The LNG ISO tank must resist a design cycle count of 108 cycles for variable temperature and pressure per design criteria to have a 20-year design lifespan. The approach of computing fatigue is comprehensively addressed in ASME Section VIII Division 2 Part 5 [20] based on elastic and equivalent stress. The study immediately refers to the smooth bar fatigue curves in Annex 3-F. In this regard, choosing the appropriate fatigue curve matching the selected building material is imperative.

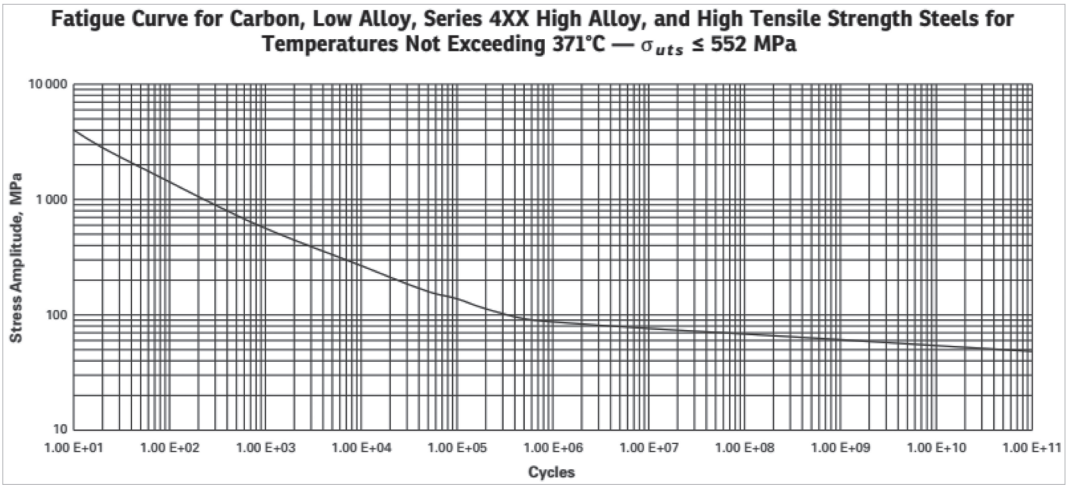

Figure 16 Fatigue curves for various types of steel [20]

Slika 16. Krivulje zamora za različite vrste čelika [20]

ASME Section VIII Division 2 Part 5 [20] provides interpolation using Equation 8 from the fatigue curve in Fig. 16.

$$Y = log\left[28.3\ E3\left(\frac{S_a}{E_T}\right)\right] \quad (8)$$

The value Y is used as an exponent to determine the allowable number of cycles X. E_T is the material's modulus of elasticity. Where the value of X for 10^y<20 is found in Equation 9.

$$X = \frac{38.1309 - 60.1705Y^2 + 25.0352Y^4}{1 + 1.80224Y^2 - 4.68904Y^4 + 2.26536Y^6} \quad (9)$$

And if the value of 10^y≥20, then X is obtained using Equation 10.

$$X = -4706.5245 + 1813.6228Y + \frac{6785.5644}{Y} - 368.12404Y^4 - \frac{5144.7345}{Y^2} + 30.708204Y^3 + \frac{1596.1916}{Y^3} \quad (10)$$

The values of the factors above can be determined by calculating the alternating equivalent stress amplitude as described in Equation 11.

$$S_{alt,k} = \frac{K_f . K_{e,k} . (\Delta S_{p,k} - \Delta S_{LT,k}) + K_{v,k} . \Delta S_{LT,k}}{2} \quad (11)$$

The fatigue penalty factor $K_{e,k}$ is the fatigue penalty factor used for the entire stress range. Since this study does not involve thermal loads, Poisson correction factor values $K_{e,k}$ and $\Delta S_{LT,k}$ can be disregarded. Therefore, Equation 11 can be written as Equation 12.

$$S_{alt,k} = \frac{K_f . K_{e,k} . \Delta S_{p,k}}{2} = S_a \quad (12)$$

In this context, S_a denotes the stress amplitude derived from calculations, $\Delta S_{p,k}$ refers to the stress range of the component and K_f is the fatigue strength reduction factor, which has a value of 1.2 as specified in ASME VIII, Division 2 [20]. The factor $K_{e,k}$ is assigned a value of 1 because $K_{e,k'}$ is less than $\Delta S_{p,k} < \Delta S_{PS}$. After acquiring all the aforementioned factors, the fatigue damage value can be calculated by dividing the number of design cycles n by the allowable cycle count N, as illustrated in Equation 13.

$$D_f = \frac{n}{N}, \text{ with } N = 10^x \quad (13)$$

The fatigue calculation results presented in Tables 6-9, encompassing both low-cycle and high-cycle tests, provide a comprehensive assessment of four models, emphasizing their structural performance under diverse conditions. A key consistency across all tests is the uniform fatigue penalty factor ($K_{e,k}$) of 1 and fatigue strength reduction factor K_f of 1.2, ensuring a standardized safety margin, alongside a constant modulus of elasticity E_T of 210,000 MPa, which underscores the material's reliable stiffness. Model D exhibits superior fatigue performance, as evidenced by its lowest stress ranges and highest permissible cycles in most tests, particularly excelling under vertical and transversal conditions. Conversely, Models A and B experience higher stress levels but maintain low damage factors, underscoring their robustness. The longitudinal test reveals a higher damage factor for Model D, indicating a need for specific design modifications to improve its performance under this loading condition.

Table 6 The fatigue calculation results for the low-cycle test
Tablica 6. Rezultati izračuna zamora za niskociklički test

Parameters	Model			
	Model A	Model B	Model C	Model D
Fatigue penalty factor $K_{e,k}$	1	1	1	1
Fatigue strength reduction factor K_f	1.2	1.2	1.2	1.2
The component stress range $\Delta S_{p,k}$ (MPa)	45.25	32.34	23.03	17.06
Computed stress amplitude S_a (MPa)	27.15	19.40	13.82	10.24
Modulus of elasticity E_T (MPa)	210,000	210,000	210,000	210,000
Stress factor Y (MPa)	0.56	0.42	0.27	0.14
Exponent for permissible No. of cycles X	18.39	24.00	30.59	35.77
The permissible design cycles N	2.47×10^{18}	9.95×10^{23}	3.92×10^{30}	5.92×10^{35}
The total number of design cycles n_k	2000	2000	2000	2000
The fatigue damage factor $D_{f,k}$	8.11×10^{-16}	2.01×10^{-21}	5.11×10^{-28}	3.38×10^{-21}

Table 7 The fatigue calculation results for the high-cycle (vertical) test
Tablica 7. Rezultati izračuna zamora za visokociklički (vertikalni) test

Parameter	Model			
	Model A	Model B	Model C	Model D
Fatigue penalty factor $K_{e,k}$	1	1	1	1
Fatigue strength reduction factor K_f	1.2	1.2	1.2	1.2
The component stress range $\Delta S_{p,k}$ (MPa)	89.70	64.55	15.65	12.46
Computed stress amplitude S_a (MPa)	53.82	38.73	9.39	7.48
Modulus of elasticity E_T (MPa)	210,000	210,000	210,000	210,000
Stress factor Y (MPa)	0.86	0.72	0.10	0.00
Exponent for permissible No. of cycles X	10.69	13.87	36.83	38.13
The permissible design cycles N	4.88×10^{10}	7.38×10^{13}	6.74×10^{36}	1.35×10^{38}
The total number of design cycles n_k	10^8	10^8	10^8	10^8
The fatigue damage factor $D_{f,k}$	2.05×10^{-2}	1.36×10^{-5}	1.48×10^{-28}	7.42×10^{-30}

Table 8 The fatigue calculation results for the high-cycle (longitudinal) test
Tablica 8. Rezultati izračuna zamora za visokociklički (uzdužni) test

Parameters	Model			
	Model A	Model B	Model C	Model D
Fatigue penalty factor $K_{e,k}$	1	1	1	1
Fatigue strength reduction factor K_f	1.2	1.2	1.2	1.2
The component stress range $\Delta S_{p,k}$ (MPa)	36.30	36.67	35.99	96.99
Computed stress amplitude S_a (MPa)	21.78	22.00	21.59	58.20
Modulus of elasticity E_T (MPa)	210,000	210,000	210,000	210,000
Stress factor Y (MPa)	0.47	0.47	0.46	0.89
Exponent for permissible No. of cycles X	21.93	21.75	22.08	10.02
The permissible design cycles N	8.47×10^{21}	5.64×10^{21}	1.20×10^{22}	1.04×10^{10}
The total number of design cycles n_k	10^8	10^8	10^8	10^8
The fatigue damage factor $D_{f,k}$	1.18×10^{-13}	1.77×10^{-13}	8.37×10^{-14}	9.63×10^{-2}

Table 9 The fatigue calculation results for the high-cycle (transversal) test
Tablica 9. Rezultati izračuna zamora za visokociklički (poprečni) test

Parameters	Model			
	Model A	Model B	Model C	Model D
Fatigue penalty factor $K_{e,k}$	1	1	1	1
Fatigue strength reduction factor K_f	1.2	1.2	1.2	1.2
The component stress range $\Delta S_{p,k}$ (MPa)	31.26	28.03	13.18	12.69
Computed stress amplitude S_a (MPa)	18.76	16.82	7.91	7.61
Modulus of elasticity E_T (MPa)	210,000	210,000	210,000	210,000
Stress factor Y (MPa)	0.40	0.36	0.03	0.01
Exponent for permissible No. of cycles X	24.63	26.72	38.03	38.12
The permissible design cycles N	4.29×10^{24}	5.30×10^{26}	1.08×10^{38}	1.30×10^{38}
The total number of design cycles n_k	10^8	10^8	10^8	10^8
The fatigue damage factor $D_{f,k}$	2.33×10^{-16}	1.89×10^{-18}	9.27×10^{-30}	$1.67\ \ 10^{-30}$

5. CONCLUSION / *Zaključak*

This study highlights the critical role of frame design in improving the durability and strength of 40-ft LNG ISO tank containers during repeated use, as per ISO 1496-3 standards. By analysing four different models, from the strong Model A to the simple Model D, the study shows that simpler designs usually have lower stress levels in frames and corners during low and high-cycle conditions. It does not affect the pressure vessel, which remains stable due to internal pressure. However, Model D shows higher stress under high-cycle longitudinal loading, indicating a risk of bending that could affect safety during transport. Model C is the best design, reducing stress in all conditions while avoiding the risks of simpler designs. Additionally, the low fatigue damage values across models suggest these structures are strong, have a long service life, and have less need for maintenance. These findings fill a gap in research on LNG ISO tanks and help improve engineering practices for safer and more efficient LNG transport. Future studies could look at factors like corrosion or temperature changes to improve design guidelines and regulations.

Author Contribution: Conceptualization, H.Y.; methodology, H.Y.; formal analysis, A.A., and D.P.; resources, H.Y.; data curation, A.A., and D.P.; writing-original draft preparation, A.A., and D.P.; writing-review and editing, O.M., and T.T.; visualization, A.A., and D.P.; supervision, H.Y.; project administration, H.Y.; Funding Acquisition, T.T. All authors have read and agreed to the published version of the manuscript.

Funding: This work was supported by the Institute for Research and Community Services (LPPM) Universitas Diponegoro under the Professor Research Scheme 2025 with contract number 222-345/UN7.D2/PP/IV/2025. The authors gratefully acknowledge the support.

Conflict of interest: The authors have no conflicts of interest.

REFERENCES / *Literatura*

[1] Mrzljak, V., Poljak, I., & Medica-Viola, V. (2017). Energy and Exergy Efficiency Analysis of Sealing Steam Condenser in Propulsion System of LNG Carrier. *Naše more*, *64* (1), 20-25. https://doi.org/10.17818/NM/2017/1.4

[2] Mrzljak, V., Poljak, I., & Žarković, B. (2018). Eksergijska analiza ventila tlaka pare kod pomorskoga porivnog postrojenja na konvencionalnom LNG tankeru. *Naše more*, *65* (1), 24-31. https://doi.org/10.17818/NM/2018/1.4

[3] Mrzljak, V., & Poljak, I. (2019). Energy Analysis of Main Propulsion Steam Turbine from Conventional LNG Carrier at Three Different Loads. *Naše more*, *66* (1), 10-18. https://doi.org/10.17818/NM/2019/1.2

[4] Fikri, M., Hendrarsakti, J., Sambodho, K., Felayati, F., Octaviani, N., Giranza, M., & Hutomo, G. (2020). Estimating Capital Cost of Small Scale LNG Carrier. *Proceedings of the 3rd International Conference on Marine Technology*, 225–229. https://doi.org/10.5220/0008542102250229

[5] Pham, V. C., Choi, J. H., Rho, B. S., Kim, J. S., Park, K., Park, S. K., Le, V. V., & Lee, W. J. (2021). A Numerical Study on the Combustion Process and Emission Characteristics of a Natural Gas-diesel Dual-fuel Marine Engine at Full Load. *Energies*, *14* (5), 1-28. https://doi.org/10.3390/en14051342

[6] Pawlak, M. (2015). Analysis of Economic Costs and Environmental Benefits of LNG as the Marine Vessel Fuel. *Solid State Phenomena*, 236, 239-246. https://doi.org/10.4028/www.scientific.net/SSP.236.239

[7] International Maritime Organization (2019). *MARPOL Annex VI*, 1-6. https://www.imo.org/en/about/conventions/pages/international-convention-for-the-prevention-of-pollution-from-ships-(marpol).aspx, Accessed at April 13th, 2025

[8] BPK (2014). *Perubahan Kedua Atas Peraturan Pemerintah Nomor 35 Tahun 2004 Tentang Kegiatan Usaha Hulu Minyak Dan Gas Bumi*. https://peraturan.bpk.go.id/

[9] Lee, K., Murakami, S., Ölçer, A. I., Dong, T., Estebanez, G., & Schönborn, A. (2024). Hydrogen enriched LNG fuel for maritime applications – A life cycle study. *International Journal of Hydrogen Energy*, 78, 333–343. https://doi.org/10.1016/j.ijhydene.2024.06.273

[10] Uemura, T., & Ishigami, K. (2018). *Formulating Policy Options for Promoting Natural Gas Utilization in the East Asia Summit Region*. Vol II (February). https://www.eria.org

[11] Institute for Essential Services Reform (2024). *Indonesia Energy Transition Outlook 2024*. www.iesr.or.id

[12] Wang, Z., & Qian, C. (2020). Strength Analysis of LNG tank Container for Trains under Inertial Force. *Journal of Physics: Conference Series*. https://doi.org/10.1088/1742-6596/1549/3/032107

[13] Xiaodong, W., & Hu, H. (2015). Stress Analysis of LNG Storage Tank for Ships under Inertial Force. *CIESC Journal*, 66, 349-353. http://dx.doi.org/10.11949/j.issn.0438-1157.20150719

[14] Cao, J., Han, M., & Qi, J. Y. (2014). The Study on Medium Filling Scheme of LNG Tank Container Impact Testing Based on ANSYS. *Advanced Materials Research*, 912-914, 869-872. https://doi.org/10.4028/www.scientific.net/AMR.912-914.869

[15] Lee, Y., Sim, I.-H., Kim, Y. S., Jung, J. H., Park, J. S., Kwon, S. H., & Jang, T. S. (2005). Experimental Study on Sloshing for Large LNGC Design. *Proceeding of International Offshore and Polar Engineering Conference*, ISOPE-I-05-274.

[16] Park, J., Jin, K., Sung, M., & Ha, M. K. (2005). Three-dimensional Sloshing Analysis of LNG Carriers In Irregular Waves. *Proceeding of The Fifteenth International Offshore and Polar Engineering Conference*, ISOPE-I-05-270.

[17] Arai, M., Makiyama, H., Cheng, L.-Y., Kumano, A., Ando, T., & Imakita, A. Numerical and Experimental Study of 3-D Sloshing in Tanks of LNG Carriers. *Proceeding of International Conference on Offshore Mechanics and Arctic Engineering*, 763-770. https://doi.org/10.1115/OMAE2006-92235

[18] Arswendy, A., & Moan, T. (2006). Sloshing Response of LNG tank. *Proceeding of 25th International Conference on Offshore Mechanics and Arctic Engineering*, 771-779. https://doi.org/10.1115/OMAE2006-92356

[19] Park, T.-H., Lee, Y.-W., Lee, H.-H., & Shin, H.-S. (2006). Qualitative Sloshing Computations for the Assessment of Membrane LNG Cargo Containment System Design. *25th International Conference on Offshore Mechanics and Arctic Engineering*, 725-729. https://doi.org/10.1115/OMAE2006-92300

[20] ASME (2019). *ASME Boiler and Pressure Vessel Code Section VIII Division 1*. ASME, New York, NY, USA.

[21] ASME (2019). *ASME Boiler and Pressure Vessel Code Section II Part D Properties*. ASME, New York, NY, USA.

[22] Muttaqie, T., Sasmito, C., Iskendar, & Kadir, A. (2022). Structural Strength Assessment of 20-ft LNG ISO Tank: An Investigation of Finite Element Analysis and ASME Design Guidance. *IOP Conference Series: Earth and Environmental Science*, 972, 012015. https://doi.org/10.1088/1755-1315/972/1/012015

[23] ISO 1496-3:2019-4. (2019). *Series 1 Freight Containers-Specification and Testing-Part 3: Tank Containers for Liquids Gases and Pressurized Dry Bulk*. https://www.iso.org/standard/67457.html

[24] Marpaung, F., Wibowo, E. T., & Harmadi, R. (2022). Desain dan Analisis Tanki ISO LNG Kapasitas 40 feet Menggunakan Teknik Finite Element Analysis. *Jurnal Asiimetrik: Jurnal Ilmiah Rekayasa & Inovasi*, 4, 163-170. https://doi.org/10.35814/asiimetrik.v4i1.2989

[25] Purnamasari, D., Tuswan, T., Muttaqie, T., Sandjaja, I., Machfudin, A., Rizal, N., Rahadi, S., Sasmito, A., Zakki, A. F., & Mursid, O. (2024). Structural Assessment of 40 ft Mini LNG ISO Tank: Effect of Structural Frame Design on the Strength Performance. *Curved Layered Strucures*, 11, 20220219. http://dx.doi.org/10.1515/cls-2022-0219

[26] Lee, D. Y., Jo, J. S., Nyongesa, A. J., & Lee, W. J. (2023). Fatigue Analysis of a 40 ft LNG ISO Tank Container. *Materials*, 16, 428. https://doi.org/10.3390/ma16010428

[27] Tuswan, T., Andrian, M., Amiruddin, W., Muttaqie, T., Sari, D. P., Bisri, A., Yuniati, Y., Soetarjo, M., Utina, M. R., & Harmadi, R. (2024). Design Improvement Using Topology Optimization for the Structural Frame Design of a 40 Ft LNG ISO Container Tank. *Designs*, *8* (2), 21. https://doi.org/10.3390/designs8020021

[28] Chandra Ariesta, R., Zubaydi, A., Ismail, A., & Tuswan, T. (2022). Identification of Damage Size Effect of Natural Frequency on Sandwich Material using Free Vibration Analysis. *Naše more*, *69* (1), 1-8. https://doi.org/10.17818/NM/2022/1.1

[29] Fahy, M., & Tiernan, S. (2001). Finite Element Analysis of ISO Tank Containers. *Journal of Materials Processing Technology*, 119, 293-298. https://doi.org/10.1016/S0924-0136(01)01034-2

[30] ISO (2019). *ISO 1161:2019-4 Series 1 Freight Containers-Corner and Intermediate Fittings – Specifications*. https://www.iso.org

[31] Prabowo, A. R., Laksono, F. B., & Sohn, J. M. (2020). Investigation of Structural Performance Subjected to Impact Loading using Finite Element Approach: Case of Ship-Container Collision. *Curved and Layered Structures*, 7, 17-28. http://dx.doi.org/10.1515/cls-2020-0002

[32] Park, Y. Il, Cho, J. S., & Kim, J. H. (2021). Structural Integrity Assessment of Independent type-C Cylindrical Tanks using Finite Element Analysis: Comparative Study using Stainless Steel and Aluminum Alloy. *Metals*, *11* (10). https://doi.org/10.3390/met11101632

[33] Alshoaibi, A. M., & Ali Fageehi, Y. (2022). 3D Modelling of Fatigue Crack Growth and Life Predictions using ANSYS. *Ain Shams Engineering Journal*, *13* (4), 101636. https://doi.org/10.1016/j.asej.2021.11.005